Contribution from the Department of Chemistry,
The University of Mississippi, University, Mississippi 38677

Electrochemical and Spectroscopic Studies of Cobalt(II) in Molten Aluminum Chloride–*N*-*n*-Butylpyridinium Chloride

C. L. HUSSEY* and T. M. LAHER

Received November 10, 1980

Absorption spectroscopy and potentiometry were used to study the coordination of Co(II) ion in the room-temperature chloroaluminate melt system aluminum chloride–*N*-*n*-butylpyridinium chloride ($AlCl_3$–BPC). Absorption spectroscopy indicated that Co(II) was tetrahedrally coordinated as the $CoCl_4^{2-}$ ion in 0.8:1 molar ratio $AlCl_3$–BPC. Potentiometric measurements on the cell $Co|Co(II)_{dil}$, BPC-rich $AlCl_3$–BPC/fritted disk/2:1 molar ratio $AlCl_3$–BPC|Al revealed a fourth-power dependence of the cell potential on the logarithm of chloride ion mole fraction consistent with the formation of $CoCl_4^{2-}$. Spectroscopic studies of Co(II) in 2:1 molar ratio $AlCl_3$–BPC melt suggested an octahedrally coordinated species, possibly $Co(Al_2Cl_7)_m^{2-m}$, with $m = 2$. Potentiometric measurements on the cell $Co|Co(II)_{dil}$, $AlCl_3$-rich $AlCl_3$–BPC/fritted disk/2:1 molar ratio $AlCl_3$–BPC|Al suggested $m > 2$. The formation constant for the reaction $Co(Al_2Cl_7)_m^{2-m} + 4Cl^- \rightleftharpoons CoCl_4^{2-} + mAl_2Cl_7^-$ was found to be 1.6×10^{46} at 36.0 °C. Voltammetric evidence was obtained that suggested that two different Co(II) species may exist in equilibrium close to the 1:1 molar ratio composition region.

Introduction

Mixtures of aluminum chloride and *N*-*n*-butylpyridinium chloride ($AlCl_3$–BPC) form a molten salt system of adjustable Lewis acidity. One of the most unusual properties of this molten salt system is that it is liquid close to room temperature over the range of compositions from 2:1 to 1:1.33 $AlCl_3$–BPC.[1] Recent studies have shown that the distribution of chloroaluminate melt species in the $AlCl_3$–BPC system is quite different from that of related $AlCl_3$–NaCl melts.[2] This species distribution can in fact be represented by a single equilibrium reaction

$$2AlCl_4^- \rightleftharpoons Al_2Cl_7^- + Cl^- \quad K_M \qquad (1)$$

with a value of $K_M \leq 3.8 \times 10^{-13}$ at 30 °C.[3]

In recent papers we reported the electrochemistry of the Cu(II)/Cu(I) and Cu(I)/Cu[4] and Fe(III)/Fe(II)[5] electrode reactions in $AlCl_3$–BPC and a closely related room-temperature chloroaluminate melt, aluminum chloride–*N*-methylpyridinium chloride. Studies with the Fe(III)/Fe(II) couple seemed to indicate that the nature of the coordination of Fe(III) in $AlCl_3$–BPC melt substantially influences the heterogeneous charge-transfer rate for the reduction of this species.[5] In order to gain further understanding about the relationship between the coordination chemistry and electrochemistry of transition-metal ions in $AlCl_3$–BPC melts, we have investigated cobalt(II). This transition-metal species has been examined in high-temeprature inorganic chloroaluminate molten salts by several research groups using a variety of techniques.[6-13] The solubility and spectroscopic characteristics of Co(II) make it an ideal probe solute with which to study the coordination of a representative d^7 transition-metal ion in $AlCl_3$–BPC melt. The data that are obtained can also be readily compared to that concerning Co(II) coordination in related inorganic chloroaluminates.

Verdieck and Yntema[6] reported a decomposition potential of 0.69 V at Pt for $CoCl_2$ in $AlCl_3$–NaCl–KCl (66–20–14 mol %) at 156 °C. Delimarskii et al.[7] reported a decomposition potential of 0.86 V for Co(II) in equimolar $AlCl_3$–NaCl at 300 °C. In addition they reported that $CoCl_2$ appears to exhibit two reduction waves.[7] A half-wave potential value of 0.51 V was reported for Co(II) in fused $AlCl_3$–NaCl–KCl (60–26–14 mol %) at a dropping mercury electrode.[8]

Spectroscopic measurements on solutions of Co(II) in molten $AlCl_3$ at 227 °C and 5.6 atm were interpreted in terms of octahedrally coordinated $Co(Al_2Cl_7)_2$.[9] Cobalt(II) spectra in fused $AlCl_3$–KCl at 300 °C indicated an octahedrally coordinated $Co(Al_2Cl_7)_2$ species in melts containing 0–42 mol % KCl and tetrahedrally coordinated $CoCl_4^{2-}$ in mixtures containing more than 49.9 mol % KCl.[10] Angell and Gruen[11] also studied the octahedral and tetrahedral coordination of Co(II) in $AlCl_3$–$ZnCl_2$ mixtures. In a recent study Nikolic and Øye[12] examined Co(II) spectra in mixtures of aluminum chloride–2-picolinium chloride ($AlCl_3$–2-PicCl) at temperatures between 100 and 180 °C.

The energetics of the Co(II) octahedral–tetrahedral coordination transformation have been determined at 300 °C for dilute mixtures of $CoCl_2$ in $AlCl_3$–LiCl, –NaCl, –KCl, –RbCl, and –CsCl.[13] These measurements were made with use of a concentration cell arrangement. The crystal structure of $Co(AlCl_4)_2$ has also been reported.[14]

Experimental Section

The preparation and purification of the $AlCl_3$–BPC melt are detailed in a previous publication.[15] Anhydrous $CoCl_2$, 99.9%, was obtained from CERAC, Inc. Samples of anhydrous $CoCl_2$ were also obtained from Alfa Products and used in some experiments.

All experiments were conducted in a dry nitrogen atmosphere inside a Kewaunee Scientific Equipment Corp. drybox equipped with a 3-cfm inert-gas purifier for removing moisture and oxygen. Cyclic voltammetry was performed with use of an AMEL Model 551 potentiostat/galvanostat equipped with an AMEL Model 566 function generator. Cyclic voltammograms were recorded with use of a Houston Model 100 X-Y recorder. Resistance compensation was applied during cyclic voltammetric measurements. The potentiostat was equipped with an AMEL Model 731 digital integrator during coulometric generation of Co(II).

The electrochemical cell and glassy-carbon working electrode, geometric area = 0.07 cm^2, employed for voltammetric measurements, were similar to those used in previous studies.[4,5] Potentiometric titration experiments were carried out in a simple two-compartment Pyrex H-cell containing a miniature Teflon-covered stir bar. A cobalt metal working electrode was fashioned from a length of 0.25-mm cobalt wire (Alfa Products, m2N7). The electrode was dipped briefly into concentrated HNO_3 followed by similar treatment with concentrated HCl. The electrode was rinsed thoroughly with distilled H_2O and

(1) Robinson, J.; Osteryoung, R. A. *J. Am. Chem. Soc.* **1979**, *101*, 323.
(2) Gale, R. J.; Gilbert, B.; Osteryoung, R. A. *Inorg. Chem.* **1978**, *17*, 2728.
(3) Gale, R. J.; Osteryoung, R. A. *Inorg. Chem.* **1979**, *18*, 1603.
(4) Hussey, C. L.; King, L. A.; Carpio, R. A. *J. Electrochem. Soc.* **1979**, *126*, 1029.
(5) Hussey, C. L.; King, L. A.; Wilkes, J. S. *J. Electroanal. Chem. Interfacial Electrochem.* **1979**, *102*, 321.
(6) Verdieck, R. G.; Yntema, L. F. *J. Phys. Chem.* **1942**, *46*, 344.
(7) Delimarskii, Yu. K.; Skobets, E. M.; Berenblyum, L. S. *Zh. Fiz. Khim.* **1948**, *22*, 1108.
(8) de Fremont, R. M.; Rosset, R.; Leroy, M. *Bull. Soc. Chim. Fr.* **1964**, 706.
(9) Øye, H. A.; Gruen, D. M. *Inorg. Chem.* **1964**, *3*, 836.
(10) Øye, H. A.; Gruen, D. M. *Inorg. Chem.* **1965**, *4*, 1173.
(11) Angell, C. A.; Gruen, D. M. *J. Inorg. Nucl. Chem.* **1967**, *29*, 2243.
(12) Nikolic, R.; Øye, H. A. *Z. Phys. Chem. (Leipzig)* **1979**, *260*, 841.
(13) Kvaal, T.; Øye, H. A. *Acta Chem. Scand.* **1972**, *26*, 1647.
(14) Ibers, J. A. *Acta Crystallogr.* **1962**, *15*, 967.
(15) Carpio, R. A.; King, L. A.; Lindstrom, R. E.; Nardi, J. C.; Hussey, C. L. *J. Electrochem. Soc.* **1979**, *126*, 1644.

0020-1669/81/1320-4201$01.25/0

Table I. Absorption Maxima and Molar Absorptivities for Co(II) in Various Molten Chloride Solvents

melt syst (mixtures, mol %)	t, °C	λ_{max}, nm (ϵ, L/mol cm) I	II	III	ref
		Tetrahedral Coordination			
pyridinium chloride	150	699 (630)	671 (570)	639 (360)	10
$AlCl_3$-KCl (49.7-50.3)	300	694 (406)	662 (395)	613 (250)	10
$AlCl_3$-BPC (44.4-55.6)	40	696 (662)	669 (593)	633 (428)	this work
		Octahedral Coordination			
$AlCl_3$	227	675	637 (76)	599	10
$AlCl_3$-KCl (64.5-35.5)	300	685	633 (73)	599	10
$AlCl_3$-2-PicCl (60-40)	140		629 (30.4)	602 (34.1)	12
$AlCl_3$-BPC (66.7-33.3)	40		630 (16.5)	600 (26.8)	this work

dried in an oven. Both the cobalt and aluminum electrodes were digested in pure melt for 24 h prior to use. Failure to pretreat the cobalt wire in the manner described resulted in an electrode that was relatively insensitive to changes in the Co(II) activity. This effect was most pronounced in acid melts. All potentials were referenced to an aluminum wire immersed in 2:1 $AlCl_3$–BPC melt, separated from the bulk melt compartment by a fine-porosity frit.

The electrochemical cell temperature was maintained to within ±0.2 °C of the desired temperature with a thermistor-controlled furnace. The furnace consisted of an insulated aluminum block containing a Vulcan Electric 150-W cartridge heater. Regulated current to power the furnace was provided by an Ace Glass temperature controller.

Absorption spectra were recorded in 1.0-cm path length quartz cells fitted with air-tight Teflon caps with use of a Cary 17 UV–vis spectrophotometer equipped with a thermostated cell compartment. The cells were filled and sealed in the drybox. Spectra were recorded against a reference blank, which consisted of melt of the appropriate composition without added solute.

Results and Discussion

Absorption Spectroscopy. Anhydrous $CoCl_2$ was readily soluble in the acidic ($AlCl_3$-rich) and basic (BPC-rich) $AlCl_3$–BPC melt. Solutions of $CoCl_2$ in basic melt were aquamarine while acidic solutions were deep blue. The visible absorption spectra of $CoCl_2$ in both acidic and basic melts at 40.0 °C are shown in Figure 1. Solutions of Co(II) obeyed the Lambert–Beer law in both the 0.8:1 and 2:1 molar ratio $AlCl_3$–BPC melts over the concentration ranges examined, i.e., $(0.5–4.0) \times 10^{-3}$ M and $1.00 \times 10^{-3}–2.0 \times 10^{-2}$ M, respectively. The absorption spectrum of $CoCl_2$ dissolved in 0.8:1 $AlCl_3$–BPC melt exhibits a band with three distinct peaks at 633, 669, and 696 nm. This spectrum is typical of tetrahedral coordination and can be attributed to the $CoCl_4^{2-}$ ion.[10,12,16] Similar coordination of Co(II) has been reported in chloride-rich $AlCl_3$–KCl at 300 °C[10] and in $AlCl_3$-2-PicCl at 140 °C.[12] The spectrum of the $CoCl_4^{2-}$ ion shown in Figure 1 is due to a transition from the $^4A_2$ ground state to the $^4T_1$ excited state with multiple components due to mixing with formally forbidden quartet–doublet transitions.[16] Absorption maxima positions and molar absorptivities for tetrahedrally coordinated Co(II) in various chloride solvents are compared in Table I. Examination of Table I shows that the absorptivities of Co(II) in molten chlorides follow a general trend of increasing with decreasing temperature. The molar absorptivity of Co(II) in 0.8:1.0 $AlCl_3$–BPC conforms with the observed trend.

The spectrum of $CoCl_2$ dissolved in 2:1 $AlCl_3$–BPC melt, shown in Figure 1, exhibits a single broad maximum at 600 nm and a small shoulder at 530 nm. The position of these peaks and the general overall appearance of the spectrum are very similar to those of spectra observed for $CoCl_2$ in $AlCl_3$-rich $AlCl_3$-2-PicCl[12] and $AlCl_3$–KCl.[10] These spectra are attributed to octahedral coordination of Co(II) by $Al_2Cl_7^-$.[9,10,12] The molar absorptivities and positions of absorption maxima of octahedrally coordinated Co(II) in molten $AlCl_3$ and several $AlCl_3$-rich chloroaluminate melts are shown in Table I for comparison. Molar absorptivities for Co(II) in 2:1 $AlCl_3$–BPC are greatly decreased over absorptivitiy values obtained in other chloroaluminate melts. Absorptivities for Co(II) in melts rich in $AlCl_3$ follow a general trend of decreasing with increasing temperature. Values obtained for Co(II) in 2:1 $AlCl_3$–BPC are consistent with this trend.

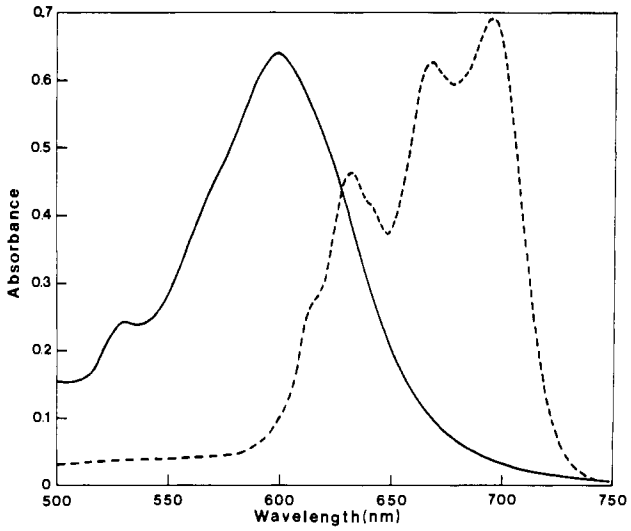

Figure 1. Absorption spectra of Co(II) in $AlCl_3$–BPC melt at 40.0 °C: (solid line) 2.04×10^{-2} M Co(II) in 2:1 $AlCl_3$–BPC melt; (dotted line) 1.02×10^{-3} M Co(II) in 0.8:1 $AlCl_3$–BPC melt.

Potentiometric Titration Studies. The nature and strength of the coordination of Co(II) were further probed in the acidic and basic $AlCl_3$–BPC melts with use of a potentiometric titration procedure. Potential measurements were made on the cell

$$Co|Co(II)_{dil}, AlCl_3\text{–BPC/fritted disk/2:1 molar ratio } AlCl_3\text{–BPC}|Al \quad (2)$$

as a function of the ratio of $AlCl_3$ to BPC in the left-hand compartment. There is at present no information about the external transport numbers of the various ionic species in room-temperature chloroaluminate melts with which to estimate the magnitude of the liquid junction potential for this cell. However, very little shift in the cyclic voltammetric half-peak potential for the ferrocenium/ferrocene couple was observed in a similar cell with wide variation in the $AlCl_3$–BPC melt composition.[1] On the basis of this indirect evidence, corrections for the liquid junction potential were assumed small and ignored.

A titration curve for potentiometric titration of Co(II) dissolved initially in 2:1 melt at 36 °C, obtained with use of the cell represented in eq 2, is shown in Figure 2. For the most part potentials obtained with this cell were stable and reproducible over the range of compositions examined, $0.44 < X_{AlCl_3} < 0.67$, where X_{AlCl_3} is the apparent mole fraction of $AlCl_3$ in the $AlCl_3$–BPC melt. However, some difficulty was

(16) Gruen, D. M.; McBeth, R. L. *Pure Appl. Chem.* **1963**, *6*, 23.

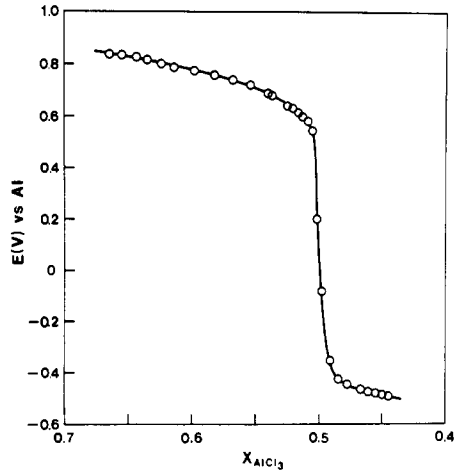

Figure 2. Potentiometric titration curve for titration of 1.45×10^{-2} M Co(II) in $AlCl_3$–BPC melt at 36.0 °C.

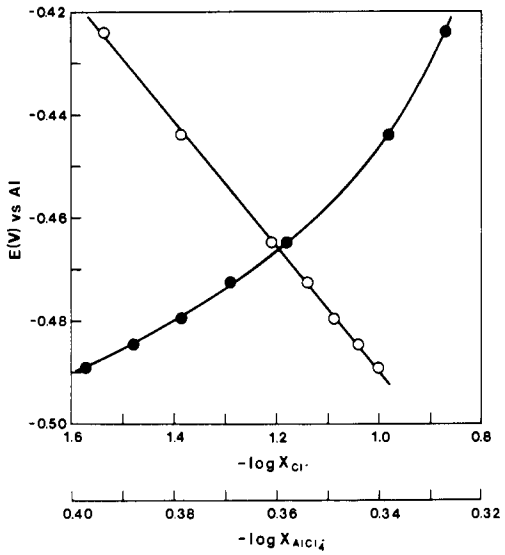

Figure 3. Dependence of the potential of the cell depicted in eq 2 on the Cl^- and $AlCl_4^-$ ion mole fractions at 36.0 °C: (○) Cl^- ion, (●) $AlCl_4^-$.

encountered during measurements in the composition range $0.49 < X_{AlCl_3} < 0.52$ due to insolubility of $CoCl_2$. A similar phenomenon has been noted previously in inorganic chloroaluminate melts in the same X_{AlCl_3} region.[13] The potential data shown in Figure 2 were compared with the mole fractions of the predominant ionic species present in the $AlCl_3$–BPC melt as a function of melt composition. Implicit in these comparisons is the assumed applicability of the Temkin model to the $AlCl_3$–BPC system. This model assumes that the activities of the various melt species are given by their ion mole fractions.

Plots of the cell potential as a function of log X_{Cl^-} and log $X_{AlCl_4^-}$, where X_{Cl^-} and $X_{AlCl_4^-}$ are the calculated mole fractions of Cl^- and $AlCl_4^-$ ions, for data obtained in the basic composition region of the melt are shown in Figure 3. To obtain data with which to construct these plots, it was necessary to vary X_{AlCl_3} in the left-hand cell compartment from 0.485 to 0.445. A linear correlation is obtained only for the plot of cell potential vs. log X_{Cl^-}. The least-squares slope of this plot, 121 ± 2 mV, was in good agreement with the theoretical 122-mV slope predicted for fourth-power dependence of the cell potential on chloride ion mole fraction at 36.0 °C according to the half-cell reaction

$$CoCl_4^{2-} + 2e^- \rightleftharpoons Co + 4Cl^- \quad (3)$$

These results are in excellent concordance with spectrscopic data presented in the previous section.

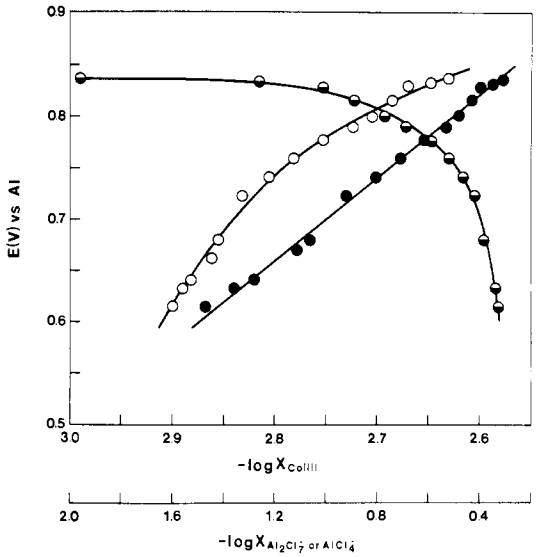

Figure 4. Dependence of the potential of the cell depicted in eq 2 on the Co(II), $Al_2Cl_4^-$, and $AlCl_4^-$ ion mole fractions at 36.0 °C: (○) Co(II) ion, (●) $Al_2Cl_7^-$ ion, (◒) $AlCl_4^-$ ion.

Similar analysis of cell potential data obtained in the composition region $0.52 < X_{AlCl_3} < 0.67$ yields more equivocal interpretation. Figure 4 shows a plot of cell potential vs. log $X_{Co(II)}$, where $X_{Co(II)}$ is the calculated mole fraction of Co(II) ion. If Co(II) ions existed in the melt in an uncomplexed form, as recently postulated for Ni(II) in acidic $AlCl_3$–BPC melt,[17] then this plot should be linear and exhibit a 30-mV slope. However, the plot shown in Figure 4 is nonlinear and exhibits a minimum slope of ca. 430 mV, which indicates that a model involving uncomplexed Co(II) ions in the acidic melt is totally inappropriate. Figure 4 also shows plots of the potential for the cell depicted in eq 2 vs. log $X_{Al_2Cl_7^-}$ and log $X_{AlCl_4^-}$, where $X_{Al_2Cl_7^-}$ and $X_{AlCl_4^-}$ are the calculated mole fractions of $Al_2Cl_7^-$ and $AlCl_4^-$ ions in the acidic melt. Inspection of Figure 4 reveals that the cell potential is linearly dependent on log $X_{Al_2Cl_7^-}$. This suggests involvement of $Al_2Cl_7^-$ ion in the coordination of Co(II) in support of the spectroscopic data described previously. However, the slope of this plot, 200 ± 5 mV, is larger than the theoretical 61-mV slope expected for dependence of the cell potential on $Al_2Cl_7^-$ ion mole fraction according to the reaction

$$Co(Al_2Cl_7)_2 + 2e^- \rightleftharpoons Co + 2Al_2Cl_7^- \quad (4)$$

The larger than theoretical slope for the plot of cell potential vs. log $X_{Al_2Cl_7^-}$ shown in Figure 4 must be interpreted with caution. It may indicate that more than two $Al_2Cl_7^-$ ions are present in the octahedral coordination sphere of Co(II) in $AlCl_3$–BPC melt. Further studies are in progress with Fe(II) and other 3d ions, which are expected to exhibit comparable coordination in acidic $AlCl_3$–BPC melt to see if similar effects are obtained.

Coordination Equilibrium Constant. The octahedral–tetrahedral coordination transformation equilibrium reaction for Co(II) in $AlCl_3$–BPC melt is represented by the expression given in eq 5, where m is an integer. The relationship between

$$Co(Al_2Cl_7)_m^{2-m} + 4Cl^- \rightleftharpoons CoCl_4^{2-} + mAl_2Cl_7^- \quad (5)$$

the potential of the cell depicted in eq 2 and X_{Cl^-} in the left-hand compartment of this cell is given by eq 6. In deriving

$$E = E_X^\circ + \frac{RT}{2F} \ln X_{CoCl_4^{2-}} - \frac{RT}{2F} \ln K_f - \frac{RT}{2F} \ln X_{Cl^-}^4 \quad (6)$$

(17) Gale, R. J.; Gilbert, B.; Osteryoung, R. A. *Inorg. Chem.* **1979**, *18*, 2723.

Table II. Potentials, Species Mole Fractions, and Calculated Formation Constants for Titration of $CoCl_2$ in Basic $AlCl_3$–BPC Melt at 36.0 °C

E, V	$10^2X_{Cl^-}$[a]	$X_{CoCl_4^{2-}}$	$10^2X_{Cl^-}$[b]	log K_f
−0.4241	2.92	1.12×10^{-3}	2.69	46.3
−0.4438	4.11	1.09×10^{-3}	3.89	46.3
−0.4647	6.19	1.04×10^{-3}	5.98	46.2
−0.4725	7.27	1.02×10^{-3}	7.07	46.2
−0.4795	8.18	9.95×10^{-4}	7.98	46.2
−0.4844	9.08	9.74×10^{-4}	8.89	46.1
−0.4890	9.95	9.53×10^{-4}	9.76	46.1

[a] Chloride ion mole fraction in excess of the 1:1 $AlCl_3$–BPC melt composition. [b] Excess chloride ion minus the amount complexed with $CoCl_2$.

Table III. Chloro Complex Formation Constants for Transition-Metal Ions in Chloroaluminate Melts

species	melt syst	t, °C	log K_f	ref
$CoCl_4^{2-}$	$AlCl_3$–LiCl	300	6.5	13
$CoCl_4^{2-}$	$AlCl_3$–NaCl	300	11.2	13
$CoCl_4^{2-}$	$AlCl_3$–CsCl	400	19.7	13
$CoCl_4^{2-}$	$AlCl_3$–BPC	36	46.2 ± 0.1	this work
$NiCl_4^{2-}$	$AlCl_3$–BPC	40	45.9	17

this expression, the activities of the various ionic species have been replaced by their ion mole fractions, $E_X°$ is the standard potential of the Co(II)/Co couple on the mole fraction scale in 2:1 $AlCl_3$–BPC melt, and K_f is the formation constant for the $CoCl_4^{2-}$ ion. Values of K_f for the process represented by eq 5 may be calculated at each value of E and X_{Cl^-} with use of eq 6 if $E_X°$ is known and $X_{CoCl_4^{2-}}$ can be estimated. Equation 6 is independent of the value of m chosen for eq 5. Estimates of $E_X°$ for the Co(II)/Co couple at 36.0 °C were obtained from the intercept of a Nernst plot. Data with which to construct this plot were acquired by careful addition of weighed portions of $CoCl_2$ to 2:1 molar ratio $AlCl_3$–BPC melt in the left-hand compartment of the cell depicted in eq 2. A plot of cell potential vs. log $X_{Co(II)}$ was linear with a slope of 0.0315 ± 0.0004 V and an intercept of 0.894 ± 0.002 V at 36.0 °C.

The observed potentials, various ion mole fractions, and calculated K_f values obtained at 36.0 °C are listed in Table II. Values of K_f for cobalt chloro complex formation in inorganic chloroaluminate melts and nickel chloro complex formation in $AlCl_3$–BPC melt are shown in Table III for comparison. The values of K_f observed in $AlCl_3$–BPC melt are larger by many orders of magnitude than those observed in inorganic chloroaluminate melts. These results are consistent with the decreased ionic field strength of the *N*-*n*-butylpyridinium cation resulting from its larger ionic radius relative to that of alkali metal cations. The reaction depicted in eq 5 is much more favorable from an electrostatic point of view since the *N*-*n*-butylpyridinium cation can exert only weak electrostatic attraction for melt chloride ion. The effect observed is quite similar to that proposed to account for the increased extent of $Al_2Cl_7^-$ ion formation in molten chloroaluminates when the cation ionic field strength is decreased.[3,18]

Voltammetry of Cobalt(II) in $AlCl_3$–BPC Melt. A cyclic voltammogram for the reduction of Co(II) in 2:1 $AlCl_3$–BPC melt at a glassy-carbon electrode is shown in Figure 5a. The reduction peak potential for deposition of cobalt metal from the 2:1 $AlCl_3$–BPC melt shifts negatively by about 160 mV for each order of magnitude increase in scan rate. In addition, the reverse scan in Figure 5a exhibits a hysteresis-like effect. Chronoamperometric current–time curves for Co(II) reduction in 2:1 $AlCl_3$–BPC exhibit maxima with induction times dependent on the applied potential, as depicted in Figure 6.

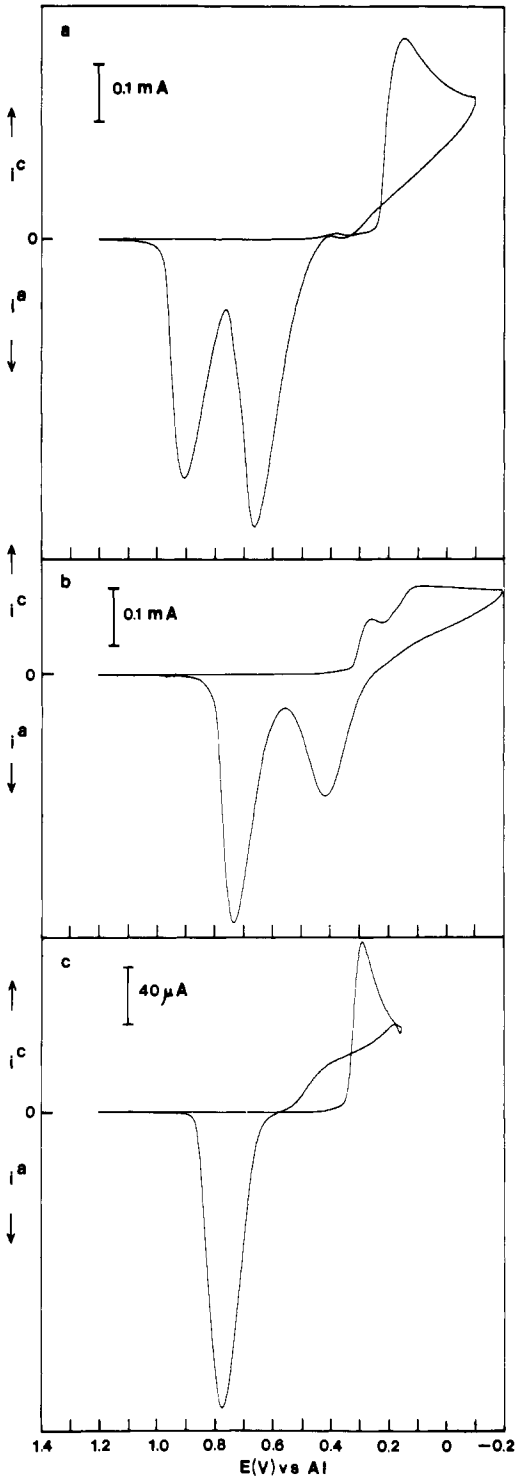

Figure 5. Cyclic voltammograms for the deposition and stripping of cobalt metal at a glassy-carbon electrode (area = 0.071 cm^2) in acidic $AlCl_3$–BPC melt at 40.0 °C; sweep rates are 0.020 V/s: (a) 2:1 $AlCl_3$–BPC melt, 5.71×10^{-2} M Co(II); (b) 1.33:1 $AlCl_3$–BPC melt, 4.15×10^{-2} M Co(II); (c) 1.14:1 $AlCl_3$–BPC melt, 3.78×10^{-2} M Co(II).

These electrochemical data suggest that deposition of cobalt metal from 2:1 $AlCl_3$–BPC melt is controlled by the rate of nucleation during the initial phases of deposit formation.[19] Similar behavior has been reported for deposition of copper[4] and aluminum[20] at glassy carbon in room-temperature chlo-

(18) Torsi, G.; Mamantov, G. *Inorg. Chem.* **1972**, *11*, 1439.

(19) Hills, G. J.; Schiffrin, D. J.; Thompson, J. *Electrochim. Acta* **1974**, *19*, 657.

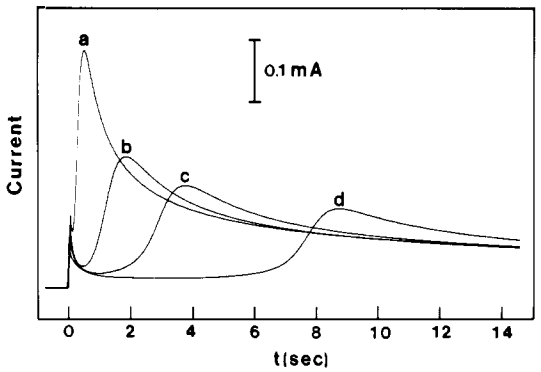

Figure 6. Current–time transients for Co(II) reduction at a glassy-carbon electrode (area = 0.071 cm^2) in 2:1 $AlCl_3$–BPC melt at 40.0 °C; Co(II) concentration was 1.26×10^{-2} M: (a) 0.050 V; (b) 0.025 V; (c) 0.0 V; (d) −0.050 V.

roaluminate melts. Two stripping peaks located at ca. 0.91 and 0.67 V, which correspond to reoxidation of material deposited on the electrode surface, are also evident in Figure 5a. The peak at 0.67 V may be due to reoxidation of aluminum codeposited with cobalt, since the voltammetric scan was extended to −0.10 V, which is very close to the potential for reduction of $Al_2Cl_7^-$ at glassy carbon at ca. −0.15 V.[20] As the melt is made less acidic by successive additions of BPC and the $Al_2Cl_7^-$ ion concentration is reduced, the peak attributed to reoxidation of codeposited aluminum at 0.67 V begins to decrease (Figure 5b), and the large featureless reduction wave observed at 0.13 V in Figure 5a begins to split into a well-defined reduction wave at 0.25 V and a less distinct wave at 0.13 V. The wave at 0.25 V increases in height with further decrease in the $Al_2Cl_7^-$ ion concentration, while the wave at 0.13 V decreases in height. Reversal of the scan after the first reduction wave diminishes the oxidation wave at 0.67 V considerably. After further decrease in the $Al_2Cl_7^-$ ion concentration, it is possible to obtain a deposition-stripping voltammogram that appears to involve only one redox process (Figure 5c).

The two reduction waves observed for Co(II) in Figure 5b may indicate that two somewhat different Co(II) species coexist in slightly acidic $AlCl_3$–BPC melt. Unfortunately it was not possible to obtain additional conclusive data supporting this premise, since the Co(II) reduction process was also complicated by nucleation phenomena and codeposition of aluminum. If the aciditiy of the melt is further decreased to the 1:1 $AlCl_3$–BPC composition, the melt becomes cloudy and some of the Co(II) precipitates from the melt, presumably, as $CoCl_2$. No reduction or reoxidation wave was observed for Co(II) in basic $AlCl_3$–BPC mixtures over the available potential range. However, the potentiometric titration data, which appear in Table II, predict that the reduction of Co(II) should be observed well within the negative limit of the BPC-rich $AlCl_3$–BPC melt at about −0.7 V. Thus Co(II) may be electroinactive at the glassy-carbon electrode when complexed as $CoCl_4^{2-}$. Similar behavior of $NiCl_4^{2-}$ in $AlCl_3$–BPC melt was recently reported.[17]

Predeposition of Cobalt Metal on Glassy Carbon. An additional feature present in the voltammogram shown in Figure 5a is a small wave at about 0.35 V. The presence of this peak was independent of the source of Co(II); i.e., the peak was present after the addition of anhydrous $CoCl_2$ from two different commercial sources or generation of Co(II) from a cobalt wire electrode by controlled-potential electrolysis. This peak was not present in pure $AlCl_3$–BPC melt prior to addition of Co(II). An expanded-scale multiple-scan cyclic voltammogram, which encompasses this reduction peak but avoids the main deposition process, is shown in Figure 7. Cyclic scans that include this reduction wave reveal an associated stripping process at about 0.8 V. Several cycles are necessary before the area of this stripping peak begins to approximate that of the original reduction process. The potential at which the stripping peak is observed is proximate to the peak for stripping of cobalt melt as shown by comparison of Figures 5 and 7.

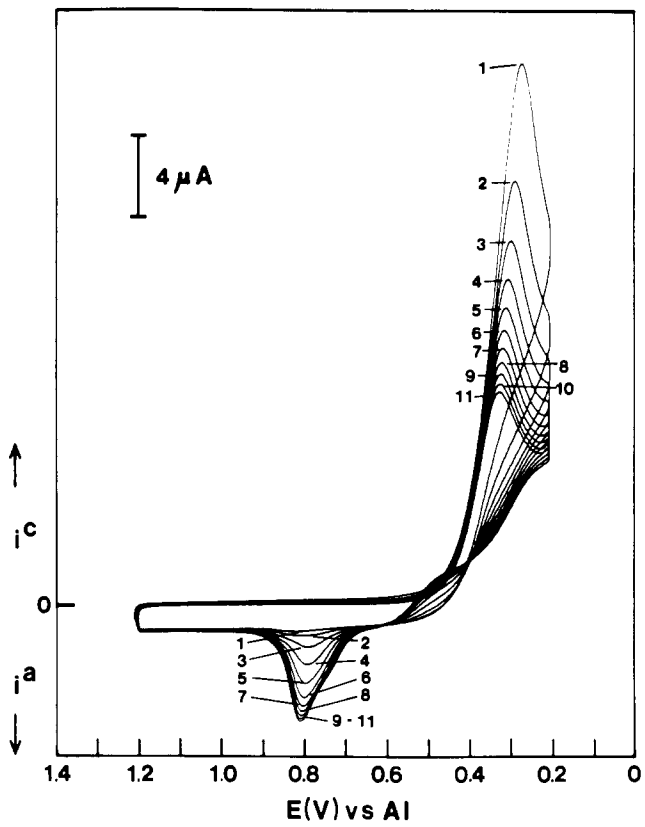

Figure 7. Multiple cyclic voltammograms of the Co(II) predeposition-stripping process at a glassy-carbon electrode (area = 0.071 cm^2) in 2:1 $AlCl_3$–BPC melt at 40.0 °C; the Co(II) concentration was 5.17×10^{-2} M and the sweep rate was 0.200 V/s. Successive scans are numbered.

Table IV. Effect of Concentration on the Predeposition of Cobalt Metal at a Glassy-Carbon Electrode

Co(II) concn, M	amt of cobalt metal, mol	% monolayer coverage[a]
12.6×10^{-3}	2.72×10^{-10}	92
21.1×10^{-3}	2.46×10^{-10}	83
30.1×10^{-3}	2.33×10^{-10}	79
51.7×10^{-3}	1.88×10^{-10}	63

[a] If it is assumed that the geometrical area of the electrode represents its true area, 2.96×10^{-10} mol of cobalt metal is required per monolayer.

Similar deposition and stripping of a monolayer or less of aluminum metal positive of the main deposition-stripping process in acidic $AlCl_3$–BPC melt was observed in previous studies and attributed to an underpotential deposition process.[20] Integration of the area under the voltammetric predeposition peak (first scan) shown in Figure 7 with respect to charge was undertaken at several concentrations of Co(II). These results are presented in Table IV and indicate that the charge under this peak may correspond to as much as one monolayer of deposited cobalt metal. Thus, deposition of cobalt metal on glassy carbon would seem to be preceded by predeposition of a monolayer of the metal. The amount of predeposited cobalt appears to recede at high concentrations of Co(II). Formation

(20) Robinson, J.; Osteryoung, R. A. *J. Electrochem. Soc.* **1980**, *127*, 122.

of a complete monolayer is most favorable at low Co(II) concentrations. This observation contrasts with results reported by Hills et al.[21] for monolayer formation during the reduction of Ni(II) and Ag(I) in LiCl-KCl eutectic. These workers reported that monolayer formation was relatively independent of the substrate ion concentration. In the present case this process could hardly be described as underpotential deposition in the thermodynamic sense, because $E_X°$ for the Co(II)/Co couple is positive of the predeposition wave by about 0.5 V. In addition, most reported $E_{1/2}$ values for Co(II) reduction in inorganic chloroaluminate melts are also significantly positive of the potential reported for this predeposition wave. A complete explanation of this phenomenon awaits further, more detailed studies.

Acknowledgment. Support of this work by a Hooker Chemical Corp. Grant of the Research Corp. and by a University of Mississippi Faculty Research Grant is gratefully acknowledged.

Registry No. BPC, 1124-64-7; $AlCl_3$, 7446-70-0; $Co(Al_2Cl_7)_2$, 37308-38-6; $CoCl_4^{2-}$, 14337-08-7.

(21) Hills, G. J.; Schiffrin, D. J.; Thompson, J. *J. Electrochem. Soc.* **1973**, *120*, 157.

Contribution from the Christopher Ingold Laboratories, University College, London WC1H OAJ, England, and the Department of Chemistry, Queen Mary College, London E1, England

Crystal Structure and Electronic, Infrared, Raman, and Resonance Raman Spectra of the Mixed-Valence, Halogen-Bridged, Anion-Chain Complexes $Cs_2[Pt^{II}(NO_2)(NH_3)X_2][Pt^{IV}(NO_2)(NH_3)X_4]$, X = Br or I

ROBIN J. H. CLARK,* MOHAMEDALLY KURMOO, ANITA M. R. GALAS, and MICHAEL B. HURSTHOUSE

Received February 19, 1981

The complexes $Cs_2[Pt^{II}(NO_2)(NH_3)X_2][Pt^{IV}(NO_2)(NH_3)X_4]$, with X = Br or I, consist of infinite, almost linear, chains in which the halogen atoms link the *trans*-$Pt(NO_2)(NH_3)X_2$ units. The crystal structures of both salts were refined within the space group *Pnam* (four $CsPt(NO_2)(NH_3)X_3$ units per unit cell) to final *R* factors of 0.036 (X = Br) and 0.038 (X = I). The chains of $[Pt^{II}(NO_2)(NH_3)X_2][Pt^{IV}(NO_2)NH_3X_4]$ are longitudinally disordered so that all Pt atom sites comprise $^1/_2Pt^{II} + {}^1/_2Pt^{IV}$ and the axial X atoms half occupy two positions ~0.6-0.8 Å apart. The key bond lengths are as follows: Pt-NH_3, 2.076 (bromide) and 2.067 Å (iodide); Pt-NO_2, 2.064 (bromide) and 2.033 Å (iodide); Pt-Br_{ax}, 2.492 Å; Pt-Br_{eq}, 2.443 Å; Pt-I_{ax}, 2.711 Å; Pt-I_{eq}, 2.631 Å. The complexes are strongly colored and highly dichroic and exhibit very rich and detailed resonance Raman spectra when irradiated within the contour of the $Pt^{II} \rightarrow Pt^{IV}$ intervalence band at 19 000 (bromide) and 12 800 cm^{-1} (iodide). In particular, for the bromide, 11 three-or-more-membered progressions were observed, for nine of which ν_1, the symmetric Br-Pt^{IV}-Br stretching mode at 178 cm^{-1}, acts as the progression-forming mode. The results imply a substantial change in the Pt-X_{ax} bond length in the intervalence state for each complex together with other smaller changes in the Pt-X_{eq} and nitro group bonds in this state.

Introduction

The electronic, infrared, Raman, and resonance Raman (RR) spectra of a variety of linear-chain, halogen-bridged complexes of platinum have now been studied,[1-6] in particular those cases in which the infinite chains are either cationic (A)

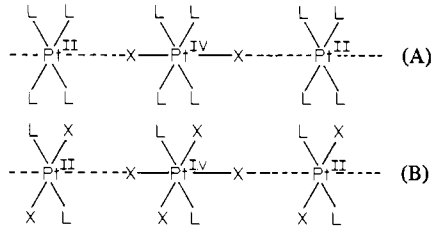

(L = neutral amine, X = Cl, Br, or I)

or neutral (B). Such complexes are deeply colored, strongly dichroic, and semiconducting along the chain axis (though insulating perpendicular thereto). The color is attributed to the axially polarized $Pt^{II} \rightarrow Pt^{IV}$ intervalence transition. Irradiation within the contour of the intervalence band leads in all cases to the appearance in the RR spectra of long progressions in which ν_1, ν(X-Pt^{IV}-X), the symmetric Pt-X stretching mode, acts as the progression-forming mode. However, few studies of anion chain complexes have yet been made and such complexes have, in general, yielded unremarkable RR spectra.[7] Two further platinum complexes, initially prepared and formulated as $Cs[Pt(NO_2)(NH_3)Br_{3.25}]$ and $Cs[Pt(NO_2)(NH_3)I_3]$ by Muraveiskaya et al.,[8,9] have recently been reformulated as class II mixed-valence complexes $Cs_2[Pt^{II}(NO_2)(NH_3)X_2][Pt^{IV}(NO_2)(NH_3)X_4]$ by Seth et al.,[10] principally on the basis of analytical, photoelectron, and electrical conductance studies. These complexes afford the opportunity for very detailed RR studies on a particular type of anion chain complex, the reformulation of which appeared to be correct on the basis of the high anisotropy of their optical absorption and electrical conductance. The present investigation is therefore concerned with (a) the determination of the crystal structure of the two nitro complexes, proving their

* To whom correspondence should be addressed at University College.

(1) Clark, R. J. H. *Ann. N.Y. Acad. Sci.* **1978**, *313*, 672 and references therein.
(2) Clark, R. J. H.; Turtle, P. C. *Inorg. Chem.* **1978**, *17*, 2526.
(3) Campbell, J. R.; Clark, R. J. H.; Turtle, P. C. *Inorg. Chem.* **1978**, *17*, 3622.
(4) Clark, R. J. H.; Kurmoo, M. *Inorg. Chem.* **1980**, *19*, 3522.
(5) Clark, R. J. H.; Kurmoo, M.; Buse, K. D.; Keller, H. J. *Z. Naturforsch. B: Anorg. Chem., Org. Chem.* **1980**, *35B*, 1272.
(6) Clark, R. J. H.; Kurmoo, M.; Keller, H. J.; Keppler, B.; Traeger, U. *J. Chem. Soc., Dalton Trans.* **1980**, 2498.
(7) Papavassiliou, G. C.; Layek, D. *Z. Naturforsch. B: Anorg. Chem., Org. Chem.* **1980**, *35B*, 676. Clark, R. J. H.; Kurmoo, M., unpublished work.
(8) Muraveiskaya, G. S.; Antokol'skaya, I. I. *Russ. J. Inorg. Chem.* **1970**, *15*, 373.
(9) Koz'min, P. A.; Surazhskaya, M. D.; Muraveiskaya, G. S.; Antokol'skaya, I. I. *Russ. J. Inorg. Chem.* **1971**, *16*, 302.
(10) Seth, P. N. A.; Underhill, A. E.; Watkins, D. M. *J. Inorg. Nucl. Chem.* **1980**, *42*, 1151.

0020-1669/81/1320-4206$01.25/0